Articles

Human Factor Xa Bound Amidine Inhibitor Conformation by Double Rotational-Echo Double Resonance Nuclear Magnetic Resonance and Molecular Dynamics Simulations

Lynda M. McDowell,*,† Margaret A. McCarrick,†,‡ Daniel R. Studelska,†,⊥ Robert D. O'Connor,† David R. Light,§ William J. Guilford,§ Damian Arnaiz,§ Marc Adler,§ Jerry L. Dallas,§ Barbara Poliks,|| and Jacob Schaefer†

Department of Chemistry, Washington University, One Brookings Drive, St. Louis, Missouri 63130, Berlex Biosciences, 15049 San Pablo Avenue, Richmond, California 94804, Department of Physics, State University of New York at Binghamton, Binghamton, New York 13902

Received May 29, 2002

Double rotational-echo double resonance (double REDOR) NMR was used to investigate the conformation of a ^{13}C-, ^{15}N-, and ^{19}F-labeled inhibitor (Berlex Biosciences compound no. ZK-806299) bound to human factor Xa. Conformationally dependent carbon−fluorine dipolar couplings were measured by $^{13}C\{^{19}F\}$ REDOR. Natural abundance carbon signals in the full-echo spectra were removed by $^{13}C\{^{15}N\}$ REDOR. Major and minor binding modes were suggested by the NMR data, but only the former had adequate signal to noise for distance determinations. Molecular dynamics simulations restrained by double-REDOR-determined intramolecular $^{13}C-^{19}F$ distances revealed two models for the dominant binding mode that are consistent with the NMR data. We conclude that ZK-806299 binds similarly to both FXa. Moreover, it appears to bind to FXa in a fashion previously demonstrated for ZK-807834, a more selective FXa inhibitor.

Introduction

Human factor Xa (FXa) is a 45 kDa enzyme belonging to the serine protease class. When complexed with membrane-associated factor Va, FXa proteolytically converts prothrombin to thrombin in the rate-limiting step of blood coagulation.[1] Recent in vivo studies demonstrate that potent FXa inhibitors are efficacious in models of both venous and arterial thrombosis without causing an excessive increase in bleeding.[2] Inhibitors having specificity for FXa over trypsin (a digestive enzyme that is also a serine protease), while maintaining selectivity against thrombin, have been reported.[3] Rotational-echo double resonance[4] (REDOR) solid-state NMR experiments and molecular dynamics (MD) simulations determined the trypsin-bound conformations of two such inhibitors.[5] For trypsin-bound inhibitor ZK-806299 (**1**), MD calculations without REDOR restraints yielded a model with an unsymmetrical inhibitor conformation, whereas calculations with REDOR restraints indicated a relatively symmetrical structure having similar $^{13}C-^{19}F$ distances to the amidino carbon and amino carbon.[5] The experiments reported here characterize the same inhibitor bound to FXa. There is only one crystal structure of a bis-(phenoxy)pyridine inhibitor bound to FXa.[6] REDOR data coupled with molecular modeling yield probable binding modes of inhibitors (like **1**) for which there are no crystal structures.

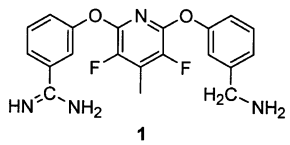

1

The complex of **1** that we examined was not crystalline. We prepared this sample using cryo- and lyoprotectants PEG 8000 and trehalose, which have been shown to maintain enzymes in their native state during freezing stress and during drying.[7] Our prior work with trypsin[5] indicated that the Ca^{2+} in our sample plus the FXa inhibitor caused sample melt-back during lyophilization. Inclusion of dextran at 1.34% (w/v) and primary and secondary drying process at low temperatures produced the fluffy cake we consider ideal. The slowly cooled protein complex is relaxed at the moment of freezing and is maintained in that state during primary drying (ice crystal sublimation) and secondary drying (removal of part of the residual liquid water always present in complex frozen material).

Experimental Methods

Solid-State NMR Sample Preparation. Human factor Xa purified from plasma was purchased from Enzyme Research Labs (South Bend, IN). The synthesis of specifically labeled **1** was described previously.[5] All other reagents were obtained from Sigma Chemical Company (St. Louis, MO). The FXa (from various lots) was thawed and combined. Except where indicated, all subsequent procedures were at ice temperature.

* To whom correspondence should be addressed. Phone: 314-935-8528. Fax: 314-935-4481. E-mail: mcdowell@wuchem.wustl.edu.
† Washington University.
‡ Current Address: Celgene Corporation, 4550 Towne Centre Court, San Diego, California 92121.
§ Berlex Biosciences.
|| State University of New York at Binghamton.
⊥ Current address: Department of Pathology and Immunology, Box 8188, Washington University School of Medicine, 660 S. Euclid Ave., St. Louis, Missouri 63110.

10.1021/jm0202324 CCC: $25.00
Published on Web 01/01/2003

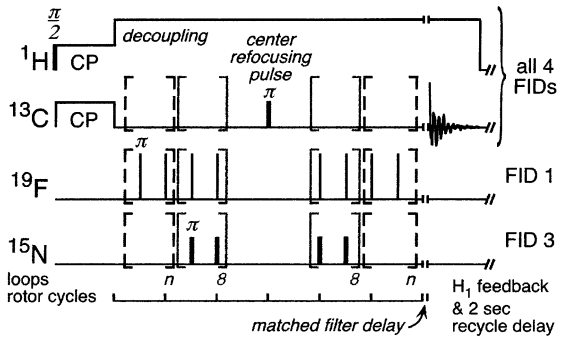

Figure 1. ^{13}C{^{15}N or ^{19}F} double REDOR pulse sequence. Each acquisition was a set of four FIDs, separated by sampling pulses for RF level control and a 2 s recycle delay. FID 1 (^{19}F dephased) and FID 2 (^{13}C full echo) had timing intervals appropriate for the 5 μs ^{19}F π pulses. FID 3 (^{15}N dephased) and FID 4 (^{13}C full echo) timing intervals were correct for the 10 μs ^{15}N π pulses. FID 2 and FID 4 gave identical spectra, as expected. Loops are shown in brackets. The dephasing π pulses used *xy* eight phase cycling[23] over four rotor cycles.

The FXa storage buffer was exchanged for 5 mM HEPES, 0.6 mM cyclamic acid (hemicalcium salt), pH 8.0. After removal of protein aggregates by centrifugation, 54.6 mg of enzyme was recovered. This was complexed with an equimolar amount of **1**.[5] After transfer to a lyophilization flask, excipients dissolved in the same buffer were added for a final volume of 20 mL. The enzyme and inhibitor were 59.4 μM in 5 mM HEPES, 0.6 mM cyclamic acid (hemicalcium salt), pH 8.0, containing 15 mM trehalose, 0.25% (w/v) PEG 8000, 0.67 mg/mL dextran (MW = 81 500), and 0.67 mg/mL dextran (MW = 488 000). This solution was supercooled by incubation at −4 °C and gradual temperature decrease to −7 °C in a low-temperature bath. After the solution was frozen, the bath temperature was lowered to −80 °C. Once this temperature was achieved, vacuum was applied to the flask to begin lyophilization. A vacuum sensor near the flask monitored sublimation. The bath temperature was raised gradually over a 6-day period until the almost completely dry cake was at room temperature. Lyophilization was continued for 2 additional days. The sample was packed, under inert conditions, into a Varian/Chemagnetics 5 mm thin-wall pencil rotor.

Double REDOR. Details of the pulse lengths, radio frequency (RF) power levels, probe, and spectrometer for 125 MHz ^{13}C{^{15}N or ^{19}F} double REDOR NMR have been published.[8] Briefly, the 2 ms matched cross-polarization transfer and dephasing pulses for ^{13}C and ^{15}N were performed at 50 kHz.[8] Proton decoupling and ^{19}F dephasing pulses were 100 kHz.[8] Custom feedback circuitry was used to stabilize both the magic-angle spinning speed (to within ±2 Hz) and the RF power levels (to within 0.2%). The sample was cooled[9] to below −6 °C during NMR experiments. The rotational resonance condition[10] was avoided by 6250 Hz magic-angle spinning.

Minor changes from the published mirror symmetric, single-refocusing pulse, double REDOR sequence[9] are shown in Figure 1. Instead of using two sequential experiments having two free induction decays (FIDs) each, the four FIDs were acquired in a single experiment (Figure 1). The ^{13}C{^{19}F} REDOR FIDs (dephased and full echo) were immediately followed by ^{13}C{^{15}N} REDOR FIDs (dephased and full echo). No REDOR evolution occurs during the single rotor cycle on either side of the center refocusing pulse. The two pairs of dephasing-pulse loops on each side of the central refocusing pulse are shown as square brackets (Figure 1). The inner pair of loops (Figure 1, solid brackets) contained 8 rotor cycles for all experiments, corresponding to 16 rotor cycles of evolution. The outer pair of loops (Figure 1, dashed brackets) contained 8, 12, or 16 rotor cycles (which added an additional 16, 24, or 32 rotor cycles of evolution, respectively). Fluorine pulses in both loops were on for ^{19}F dephasing (FID 1). Only the inner-loop pulses were turned on for ^{15}N dephasing (FID 3) to selectively dephase signals from ^{13}C within 2 Å of a ^{15}N label. Neither ^{19}F nor ^{15}N pulses were on during accumulation of the full-echo signals (FID 2 and FID 4). Total evolution time was the same for all four FIDs.[9]

To increase sensitivity, the two full-echo spectra were summed. Each dephased spectrum was multiplied by 2 and subtracted from the summed full-echo spectrum to create the REDOR difference spectra. The REDOR difference spectra contain signals only from ^{13}C that are dipolar-coupled to either ^{15}N or ^{19}F. The ^{13}C{^{15}N} difference spectrum (ΔS) shows the ^{13}C signals of **1** without interference from natural abundance signals in the protein. It is the reference for distance determinations using ^{13}C{^{19}F} ΔS. To simplify data analysis, the first spinning sidebands (ssb) of the REDOR difference spectra were folded into the centerbands.[11] The folded difference spectra were fit by Gaussians (Kaleidagraph, Synergy Software, Reading, PA; error bars are included in fit output) and integrated (MacNMR, Tecmag, Inc. Houston, TX; no error analysis available). When parameters consistent with the experiments were used, Simpson[12] simulations with and without ^{19}F homonuclear coupling (1006 Hz) had a maximum deviation of 3% from each other. Because 3% is small relative to the experimental error, we used three spins (observed ^{13}C and two ^{19}F dephasing spins) with no homonuclear coupling in our REDOR dephasing calculations.[13]

Computational Methods. REDOR-constrained models were built using the FXa catalytic chain coordinates[14] and conformations of **1** matching trypsin models **2a** and **2b**.[5] Computational methods were similar to those used for trypsin models[5] except for these minor changes: (i) no chloride counterions were added; (ii) the temperature coupling constant for the protein was 0.1 ps; (iii) the half-harmonic restraints on the water cap were 0.5 kcal mol^{-1} Å^{-2}; (iv) restraints of 10 kcal mol^{-1} Å^{-2} were placed on the two hydrogen bonds from the S1 amidine to the carboxy group of Asp 189 (chymotrypsin numbering scheme) to keep the inhibitor in the pocket. The two starting models converged after 1 ns of MD. To generate the other allowed inhibitor conformation, the phenyl ring in the S4 pocket was flipped to point the *m*-methylamino group toward Phe174 instead of toward Tyr99 and MD was repeated. Theoretical REDOR dephasing curves[13] for the preliminary models were calculated and compared with the experimental data. The ^{13}C−^{19}F distance restraints were adjusted to improve the match of the calculated dephasing with the experimental data. A second cycle of MD (500 ps) yielded models whose calculated dephasing curves agreed with the data within experimental error.

Results and Discussion

Line Assignments and REDOR Dephasing. The 125 MHz ^{13}C{^{15}N or ^{19}F} REDOR spectra of the FXa complex of **1** (FXa/**1**) with 40 rotor cycles of dipolar evolution are shown in Figure 2. The ^{15}N labels allow separation of labeled ^{13}C signals from the natural-abundance ^{13}C background (Figure 2, center spectrum and upper left inset). The 164.4 and 45 ppm peaks have line widths of 1.8 and 2.7 ppm, respectively (Figure 2, center). They are assigned to amidine and amine carbons of **1** in the S1 and S4 binding sites of FXa, respectively. The broad shoulder of the amidine signal (Figure 2, upper left) is difficult to quantitate because several combinations of position and width give satisfactory fits. When a 2.1 ppm line centered at 168 ppm was used and when two Gaussians were fitted, the amidine shoulder accounted for about 30% of the amidine signal. By analogy to the trypsin/symmetric inhibitor results,[5] this implies that about 30% of the asymmetric inhibitors complexed to FXa adopt a second conformation that perturbs the chemical shift of the amidine. One possibility is that the methylamino group binds in the S1′ pocket, where it could form a hydrogen bond with Ser195. Although there is no precedent for

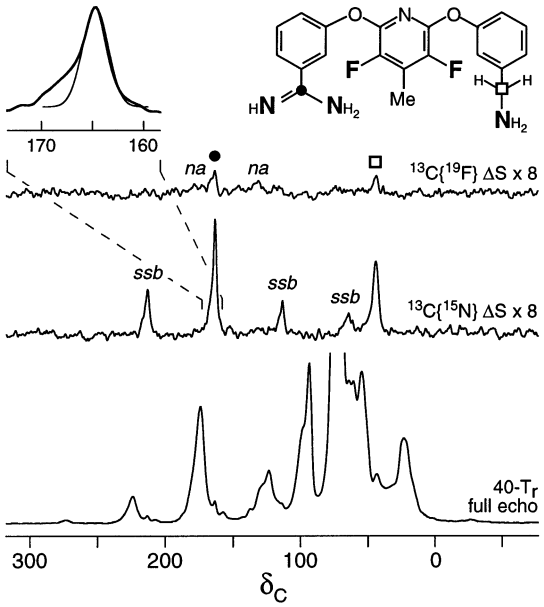

Figure 2. 125 MHz $^{13}C\{^{15}N$ or $^{19}F\}$ REDOR spectra of FXa/**1**. The dipolar evolution time was 6.4 ms (40 rotor cycles × 0.16 ms rotor period). The solid circle indicates the amidine ^{13}C label position, and the amine ^{13}C label is indicated by an open square (upper right inset). The labeled nitrogens are in boldface. The full-echo spectrum (bottom) contains signals from both the specifically labeled ^{13}C of **1** and the 1.1% naturally occurring ^{13}C in FXa and **1**. The unwanted background signals are suppressed in the $^{13}C\{^{15}N\}$ REDOR difference spectrum (middle). The smaller broad component of the amidine carbon centerband is more visible when the scale is expanded (thick line, upper left inset). The single Gaussian used for data fitting is also shown (thin line, upper left inset). The ^{13}C label intensities in the $^{13}C\{^{19}F\}$ REDOR difference spectrum (top) depend on the $^{13}C-^{19}F$ distances and the relative geometry of the two ^{19}F of the central ring with respect to the ^{13}C. Molecular models of FXa/**1** provided both distances and geometries that were consistent with the NMR data (see Figure 4). For each of the four FIDs (see Experimental Methods), 211 220 scans were accumulated.

this type of binding in FXa, it has been observed for inhibitors of the homologous proteins thrombin (1GJ4[15]) and urokinase (1GJ7[15]). The amine carbon has an even broader (4 ppm) shoulder at 50 ppm. While the amine shoulder is consistent with a second binding mode (i.e., the amine in the S1′ site), this shoulder could also arise if both orientations of the amine in the S4 site indicated by our modeling are populated (see below).

The $^{13}C\{^{19}F\}$ Δ*S* (Figure 2, top) contains signals from all carbons within about 12 Å of a ^{19}F. This includes the natural-abundance ^{13}C in **1** as well as in FXa. We assign the peaks at 133 and 146 ppm (the latter designated in Figure 2, top, by "na") to the natural-abundance ^{13}C aromatic carbons of **1** and to the (7 to 10) ^{13}C carbons in aromatic amino acids of FXa. (The variability is due to the choice of model; cf, below.) The broad peak centered at 178 ppm (also designated in Figure 2, top, by "na") is due to the (29 to 37) natural-abundance ^{13}C carbonyl carbons in FXa that should be within 12 Å of a ^{19}F. By contrast, the $^{13}C\{^{15}N\}$ Δ*S* (Figure 2, middle) shows no peak at 178 ppm, indicating a clean selection of the labeled inhibitor over natural-abundance ^{13}C. The only sign of natural-abundance ^{13}C contributions to the $^{13}C\{^{15}N\}$ Δ*S* is in the width of the amidine ^{13}C second ssb at 65 ppm (Figure 2, middle).

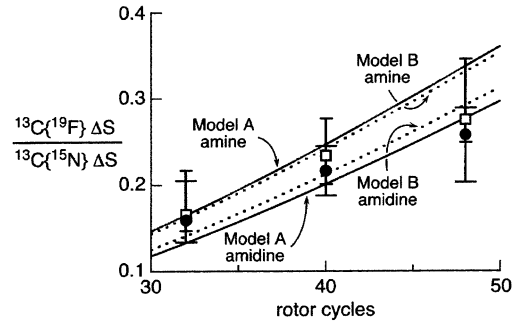

Figure 3. $^{13}C\{^{19}F\}$ REDOR dephasing for FXa/**1**. The closed circles (and wider error bars) show the experimental data (and associated uncertainty) for the amidine carbon. The open squares (and narrower error bars) show the data for the amine carbon. The solid and dotted lines are the calculated dephasing curves for models A and B (Figure 4), respectively.

This sideband is broader and larger than expected. We suspect that some of the natural-abundance ^{13}C that gives rise to the large FXa α-carbon peak (Figure 2, bottom) also contributes to the 65 ppm $^{13}C\{^{15}N\}$ Δ*S*. For this reason and because there is no signal at 65 ppm in the $^{13}C\{^{19}F\}$ Δ*S* (Figure 2, top), the amidine ^{13}C second ssb was not included in distance calculations. For the center bands and first ssb, in the unlikely event that FXa natural-abundance ^{13}C had the same chemical shift as a ^{13}C label in **1** and was also close to a ^{19}F of **1**, its $^{13}C\{^{19}F\}$ Δ*S* could not be distinguished from that due to **1.** The size of this error cannot exceed 1% of the full-echo signal (Figure 2, bottom) at the frequencies specified by the $^{13}C\{^{15}N\}$ Δ*S* spectrum (Figure 2, center). An error of this size is negligible compared to the error arising from the experimental signal to noise.

The ($^{13}C\{^{19}F\}$ Δ*S*)/($^{13}C\{^{15}N\}$ Δ*S*) values for FXa/**1** at multiple evolution times are shown in Figure 3. The amine carbon has slightly higher values than the amidine carbon in FXa/**1** (the reverse is true in trypsin/**1**[5]), but otherwise, the FXa/**1** and trypsin/**1** results are similar. These differences translate into small distance differences (≤0.4 Å) between the complexes of **1** with FXa and trypsin. Although the amidine carbon and amine carbon signals in the $^{13}C\{^{15}N\}$ Δ*S* have two components (Figure 2, center and upper left inset), the corresponding signals in the $^{13}C\{^{19}F\}$ Δ*S* were too weak for reliable fitting to two Gaussians. Instead, the peak position and width of the larger Gaussian (Figure 2, upper left, thick line) were used for single Gaussian fits. The reported $^{13}C\{^{19}F\}$ Δ*S*/$^{13}C\{^{15}N\}$ Δ*S* ratios (Figure 3) are an average of (i) integration over the entire amidine or amine ^{13}C signal and (ii) single Gaussian fits that exclude the smaller, broad components of both lines (Figure 2). The two methods yield ratios that agree within the signal to noise of the data.

The error bars (Figure 3) show the uncertainty range from the Gaussian fits only. At 40 rotor cycles (Figure 3), the data averages appear centered within the error bars because integration and Gaussian fitting gave nearly the same values. For the 32 and 48 rotor-cycle experiments, however, the agreement between integration and Gaussian fitting was not as good, so the displayed (Gaussian only) error ranges appear slightly skewed from the data averages.

The amine$-^{13}C$ peak in FXa/**1** has a shorter T_2 relaxation time (5.3 ± 0.1 ms) than was observed in

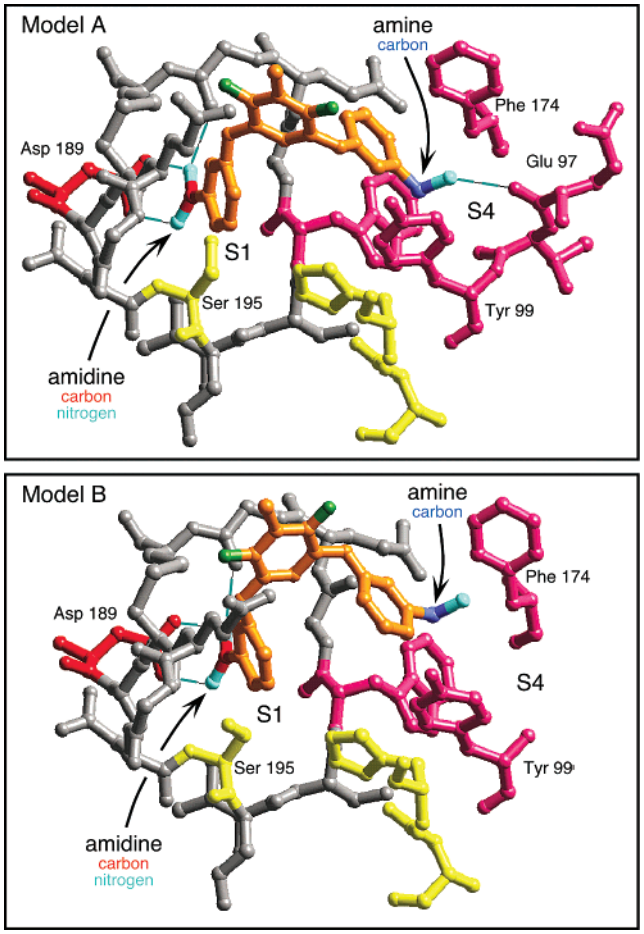

Figure 4. Two molecular models of the binding sites of FXa/**1**. Unlabeled atoms of **1** are orange. The stable isotope label sites of **1** are color-coded: fluorine, green; amidine carbon, red; amine carbon, light-blue; nitrogen, aqua. Amino acid residues in the S4 pocket of FXa are pink. FXa side chains are labeled using the chymotrypsin numbering scheme. The solid and dotted lines in Figure 3 are the calculated REDOR dephasing curves for models A and B, respectively.

trypsin/**1** (12.5 ± 1.9 ms).[5] The T_2 relaxation times of the amidine−^{13}C peak in FXa/**1** (8.1 ± 1.1 ms) and trypsin/**1** (9.1 ± 0.8 ms)[5] are similar. Both smaller sample size and faster T_2 relaxation for the amine carbon peak reduced the sensitivity of REDOR experiments for FXa/**1**. Thus, even with the higher magnetic field used in the experiments on FXa/**1**, more scans were required than for the experiments on trypsin/**1** to achieve comparable signal to noise.[5]

Modeling of the Inhibitor in FXa and Comparison with Trypsin Binding Models. Two models (designated A and B) with the amidine-carbon of **1** in the S1 binding site of FXa that are consistent with the double-REDOR NMR data are shown in Figure 4. The biggest difference between the models is the orientation of the (aminomethyl)phenyl moiety. The ^{13}C−^{19}F distances of **1** in FXa models A and B are given in Table 1.

The two models of trypsin/**1** arise from the amine group interacting with polar areas at either the top or the bottom of S4.[5] The trypsin-bound inhibitor structures, when applied to FXa, converged after dynamics and minimization. This is understandable: In FXa, the top of S4 is hydrophobic (Phe 174), so the amine prefers the bottom. The bottom of S4 in FXa (Glu 97 and Tyr 99) is even more electronegative than in trypsin (carbonyls of Thr 98 and Asn 97). The strong electronegative region of the FXa S4 pocket attracts basic groups.

Table 1. ^{13}C−^{19}F Distances in REDOR-Restrained Models of **1** Bound to Factor Xa

	^{13}C−^{19}F distance (Å)			
	model A		model B	
^{19}F	proximal	distal	proximal	distal
amidine ^{13}C	7.60	9.87	7.55	9.83
amine ^{13}C	7.26	9.89	7.30	9.56

The amine in both FXa models is perpendicular to the phenyl ring, facing up toward the solvent. This allows some solvent access to the amino groups while still partially burying the hydrophobic benzyl portions in the hydrophobic S4 pocket. In FXa/**1** model A (Figure 4, top), the amine of **1** is hydrogen bonded to the carbonyl of Glu 97. This hydrogen bond appears in 1EZQ,[16] but is not present in other published structures of FXa inhibitors, including our trypsin/**1** models.[5] Although the amino group in FXa/**1** model B (Figure 4, bottom) lacks a direct hydrogen bond, this group is in nearly the same position as in model A. The NH_3^+ to O distance is 2.8 Å in model A and 4.2 Å in model B. The overall architecture is similar to the crystal structures of the most potent (<1 nM) factor Xa inhibitors (1FJS,[6] 1EZQ,[16] 1KSN,[17] 1MQ5, 1MQ6[18]).

Other binding modes could exist which are also consistent with the experimental restraints. Nevertheless, crystal structures of trypsin complexed with other dibasic inhibitors have displayed binding modes similar to those shown in Figure 4.[19] Coordinates for the two FXa/**1** models have been deposited in the Brookhaven Protein Data Bank[20] with identification code 1MSX.

Properties of the S1 and S4 Binding Sites. Structure−activity data are available from a number of FXa inhibitor templates containing arylamidines. In general, (i) there is flexibility with respect to the nature of the second basic group, and (ii) substitution of the amidine group presumed to bind in the S1 pocket results in several orders of magnitude loss of potency.[3a,b,21] The difficulty in predicting the S4 preference from the analysis of substrate cleavage sites (in which glutamic acid is found several times) has been discussed.[22] Basic-group binding to the hydrophobic "cation hole" at S4 has been seen in the crystal structures of other small-molecule inhibitors of factor Xa.[6,18,22] The importance of the alignment of the salt bridge between the benzamidine and Asp189[6] strongly suggests that the binding mode(s) of compound **1** to FXa will preserve this critical interaction. We conclude that **1** binds similarly to both FXa and trypsin, and binds to FXa in the same general manner as revealed in the X-ray structure of the more selective inhibitor ZK-807834.[6]

Acknowledgment. This work was supported in part by NIH Grant GM40634 (J.S.). The authors thank Marc Whitlow for reviewing the manuscript.

References

(1) The role of factor Xa in the blood coagulation cascade is described in several review articles such as the following. (a) Mann, K. G.; Nesheim, M. E.; Church, W. R.; Haley, P.; Krishnaswamy, S. Surface-Dependent Reactions of the Vitamin K-Dependent Enzyme Complexes. *Blood* **1990**, *76*, 1−16. (b) Davie, E. W.;

Fujikawa, K.; Kisiel, W. The Coagulation Cascade: Initiation, Maintenance, and Regulation. *Biochemistry* **1991**, *30*, 10363−10370. (c) Butenas, S.; Mann, K. G. Blood Coagulation. *Biochemistry (Moscow)* **2002**, *67*, 3−12. (d) Rai, R.; Sprengeler, P. A.; Elrod, K. C.; Young, W. B. Perspectives on Factor Xa Inhibition. *Curr. Med. Chem.* **2001**, *8*, 101−119. (e) Dahlback, B. Blood Coagulation. *Lancet* **2000**, *355*, 1627−1632.

(2) (a) Sullivan, M.; Morser, J.; Light, D.; Guilford, W.; Vergona, R.; Hermann, M.; White, K.; Phillips, G.; Davey, D.; Morrissey, M.; Fredrich, M.; Baldus, B. The Efficacy and Safety of BX-8107834, a Potent, Selective Factor Xa Inhibitor, in Animal Models. *FASEB J.* **1998**, *12*, A719. (b) Abendschein, D. R.; Baum, P. K.; Martin, D. J.; Vergona, R.; Post, J.; Rumennik, G.; Sullivan, M. E.; Eisenberg, P. R.; Light, D. R. Effects of ZK-807834, a Novel Antagonist of Factor Xa, on Thrombosis Progression in Rabbits. *J. Cardiovasc. Pharmacol.* **2000**, *35*, 796−805. (c) Abendschein, D. R.; Baum, P. K.; Verhallen, P.; Eisenberg, P. R.; Sullivan, M. E.; Light, D. R. A Novel Synthetic Inhibitor of Factor Xa Decreases Early Reocclusion and Improves 24 Hour Patency after Coronary Fibrinolysis in Dogs. *J. Pharmacol. Exp. Ther.* **2001**, *296*, 1−6.

(3) (a) Phillips, G. B.; Buckman, B. O.; Davey, D. D.; Eagen, K. A.; Guilford, W. J.; Hinchman, J.; Ho, E.; Koovakkat, S.; Liang, A.; Light, D. R.; Mohan, R.; Ng, H. P.; Post, J. M.; Shaw, K. J.; Smith, D.; Subramanyam, B.; Sullivan, M. E.; Trinh, L.; Vergona, R.; Walters, J.; White, K.; Whitlow, M.; Wu, S.; Xu, W.; Morrissey, M. M. Discovery of *N*-[2-[5-[Amino(imino)methyl]-2-hydroxyphenoxy]-3,5-difluoro-6-[3-(4,5-dihydro-1-methyl-1*H*-imidazol-2-yl)phenoxy]pyridin-4-yl]-*N*-methylglycine (ZK-807834): A Potent, Selective, and Orally Active Inhibitor of the Blood Coagulation Enzyme Factor Xa. *J. Med. Chem.* **1998**, *41*, 3557−3562. (b) Guilford, W.; Shaw, K.; Dallas, J.; Koovakkat, S.; Lee, W.; Liang, A.; Light, D.; McCarrick, M. A.; Whitlow, M.; Ye, B.; Morrissey, M. M. Synthesis, Characterization, and Structure−Activity Relationships of Amidine-Substituted (Bis)benzylidenecycloketone Olefin Isomers as Potent and Selective Factor Xa Inhibitors. *J. Med. Chem.* **1999**, *42*, 5415−5425. (c) Light, D. R.; Guilford, W. J. Discovery of the Factor Xa Inhibitor, ZK 807834 (CI-1031). *Curr. Top. Med. Chem.* **2001**, *1*, 121−136.

(4) (a) Gullion, T.; Schaefer, J. Rotational-Echo Double-Resonance NMR. *J. Magn. Reson.* **1989**, *81*, 196−200. (b) Gullion, T.; Schaefer, J. Detection of Weak Heteronuclear Dipolar Coupling by Rotational-Echo Double-Resonance Nuclear Magnetic Resonance. *Adv. Magn. Reson.* **1989**, *13*, 57−83.

(5) McDowell, L. M.; McCarrick, M. A.; Studelska, D. R.; Guilford, W. J.; Arnaiz, D.; Dallas, J. L.; Light, D. R.; Whitlow, M.; Schaefer, J. Conformations of Trypsin-Bound Amidine Inhibitors of Blood Coagulant Factor Xa by Double REDOR NMR and MD Simulations. *J. Med. Chem.*, **1999**, *42*, 3910−3918.

(6) Adler, M.; Davey, D. D.; Phillips, G. B.; Kim, S.-H.; Jancarik, J.; Rumennik, G.; Light, D. R.; Whitlow, M. Preparation, Characterization, and the Crystal Structure of the Inhibitor ZK-807834 (CI-1031) Complexed with Factor Xa. *Biochemistry* **2000**, *39*, 12534−12542.

(7) Arakawa, T.; Prestrelski, S. J.; Kenney, W. C.; Carpenter, J. F. Factors Affecting Short-Term and Long-Term Stabilities of Proteins. *Adv. Drug Delivery Rev.* **2001**, *46*, 307−326.

(8) Li, Y.; Poliks, B.; Cegelski, L.; Poliks, M.; Gryczynski, Z.; Piszczek, G.; Jagtap, P. G.; Studelska, D. R.; Kingston, D. G. I.; Schaefer, J.; Bane, S. Conformation of Microtubule-Bound Paclitaxel Determined by Fluorescence Spectroscopy and REDOR NMR. *Biochemistry* **2000**, *39*, 281−291.

(9) Beusen, D. D.; McDowell, L. M.; Slomczynska, U.; Schaefer, J. Solid-State Nuclear Magnetic Resonance Analysis of the Conformation of an Inhibitor Bound to Thermolysin. *J. Med. Chem.* **1995**, *38*, 2742−2747.

(10) Raleigh, D. P.; Levitt, M. H.; Griffin, R. G. Rotational Resonance in Solid-State NMR. *Chem. Phys. Lett.* **1988**, *146*, 71−76.

(11) McDowell, L. M.; Lee, M.; McKay, R. A.; Anderson, K. S.; Schaefer, J. Intersubunit Communication in Tryptophan Synthase by Carbon-13 and Fluorine-19 REDOR NMR. *Biochemistry* **1996**, *35*, 3328−3334.

(12) Bak, M.; Rasmussen, J. T.; Nielsen, N. C. SIMPSON: A General Simulation Program for Solid-State NMR Spectroscopy. *J. Magn. Reson.* **2000**, *147*, 296−330.

(13) Goetz, J. M.; Schaefer, J. REDOR Dephasing by Multiple Spins in the Presence of Molecular Motion. *J. Magn. Reson.* **1997**, *127*, 147−154.

(14) Kamata, K.; Kawamoto, H.; Honma, T.; Iwama, T.; Kim, S.-H. Structural Basis for Chemical Inhibition of Human Blood Coagulation Factor Xa. *Proc. Natl. Acad. Sci. U.S.A.* **1998**, *95*, 6630−6635 (code 1xka).

(15) Katz, B. A.; Sprengeler, P. A.; Luong, C.; Verner, E.; Elrod, K.; Kirtley, M.; Janc, J.; Spencer, J. R.; Breitenbucher, J. G.; Hui, H.; McGee, D.; Allen, D.; Martelli, A.; Mackman, R. L. Engineering Inhibitors Highly Selective for the S1 Sites of Ser190 Trypsin-like Serine Protease Drug Targets. *Chem. Biol.* **2001**, *8*, 1107−1121.

(16) Maignan, S.; Guilloteau, J. P.; Pouzieux, S.; Choi-Sledeski, Y. M.; Becker, M. R.; Klein, S. I.; Ewing, W. R.; Pauls, H. W.; Spada, A. P.; Mikol, V. Crystal Structures of Human Factor Xa Complexed with Potent Inhibitors. *J. Med. Chem.* **2000,** *43*, 3226−3233.

(17) Guertin, K. R.; Gardner, C. J.; Klein, S. I.; Zulli, A. L.; Czekaj, M.; Gong, Y.; Spada, A. P.; Cheney, D. L.; Maignan, S.; Guilloteau, J.-P.; Brown, K. D.; Colussi, D. C.; Chu, V.; Heran, C. L.; Morgan, S. R.; Bentley, R. G.; Dunwiddie, C. T.; Leadley, R. J.; Pauls, H. W. Optimization of the Beta-Aminoester Class of Factor Xa Inhibitors. Part 2: Identification of Fxv673 as a Potent and Selective Inhibitor with Excellent in Vivo Anticoagulant Activity. *Bioorg. Med. Chem. Lett.* **2002**, *12*, 1671−1674.

(18) Adler, M.; Kochanny, M. J.; Ye, B.; Rumennik, G.; Light, D. R.; Biancalana, S.; Whitlow M. Crystal Structures of Two Potent Nonamidine Inhibitors Bound to Factor Xa. *Biochemistry*, in press.

(19) Whitlow, M.; Arnaiz, D.; Buckman, B. O.; Davey, D. D.; Griedel, B.; Guilford, W. J.; Koovakkat, S. K.; Liang, A.; Mohan, R.; Phillips, G. B.; Seto, M.; Shaw, K. J.; Xu, W.; Zhao, Z.; Xu, W. Z.; Light, D. R.; Morrissey, M. M. Crystallographic Analysis of Potent and Selective Factor Xa Inhibitors Complexed to Bovine Trypsin. *Acta Crystallogr.* **1999**, *D55*, 1395−1404.

(20) Berman, H. M.; Westbrook, J.; Feng, Z.; Gilliand, G.; Bhat, T. N.; Weissig, H.; Shindyalov, I. N.; Bourne, P. E. The Protein Data Bank. *Nuclei Acids Res.* **2000**, *28*, 235−242.

(21) (a) Ng, H. P.; Buckman, B. O.; Eagen, K. A.; Guilford, W. J.; Kochanny, M. J.; Mohan, R.; Shaw, K. J.; Wu, S. C.; Lentz, D.; Liang, A.; Trinh, L.; Ho, E.; Smith, D.; Subramanyam, B.; Vergona, R.; Walters, J.; White, K. A.; Sullivan, M. E.; Morrissey, M. M.; Phillips, G. B. Design, Synthesis, and Biological Activity of Novel Factor Xa Inhibitors: 4-Aryloxy Substituents of 2,6-Diphenoxypyridines. *Bioorg. Med. Chem.* **2002**, *10*, 657−66. (b) Hirayama, F.; Koshio, H.; Katayama, N.; Kurihara, H.; Taniuchi, Y.; Sato, K.; Hisamichi, N.; Sakai-Moritani, Y.; Kawasaki, T.; Matsumoto, Y.; Yanagisawa, I. The Discovery of YM-60828: A Potent, Selective and Orally-Bioavailable Factor Xa Inhibitor. *Bioorg. Med. Chem.* **2002**, *10*, 1509−1523. (c) Maignan, S.; Mikol, V. The Use of 3D Structural Data in the Design of Specific Factor Xa Inhibitors. *Curr. Top. Med. Chem.* **2001**, *1*, 161−74.

(22) Brandstetter, H.; Kuhne, A.; Bode, W.; Huber, R.; von der Saal, W.; Wirthensohn, K.; Engh, R. A. X-ray Structure of Active Site-Inhibited Clotting Factor Xa. Implications for Drug Design and Substrate Recognition. *J. Biol. Chem.* **1996**, *22*, 29988−29992.

(23) Gullion, T.; Baker, D. B.; Conradi, M. S. New, Compensated Carr−Purcell Sequences. *J. Magn. Reson.* **1990**, *89*, 479−484.

JM0202324